Marked Structural Differences of the Mcg Bence-Jones Dimer in Two Crystal Systems†

Enrique E. Abola,‡ Kathryn R. Ely, and Allen B. Edmundson*

ABSTRACT: When crystallized in water, the Bence-Jones (light-chain) dimer from the patient Mcg assumes a different overall conformation from that seen in crystals grown in ammonium sulfate. In water the protein crystallizes in the orthorhombic space group $P2_12_12$, with a = 72.6, b = 81.9, and c = 71.0 Å. In ammonium sulfate the space group is $P3_121$ (trigonal), with a = 72.3 and c = 185.9 Å. The crystallographic asymmetric unit is the dimer (M_r 46000) in both cases. The structure of the dimer in the trigonal form was previously determined to 2.3-Å resolution, and an atomic model was built with the aid of the complete amino acid sequence [Fett, J. W., & Deutsch, H. F. (1974) *Biochemistry 13*, 4102]. The orthorhombic form diffracts to even higher resolution, and 2.0-Å data have been collected for the native protein. The structure has been solved to 6.5-Å resolution by the multiple isomorphous derivative method. As in the trigonal form, each light chain consists of V ("variable") and C ("constant") globular domains connected by an extended and flexible segment of polypeptide chain (the "switch" region). A comparison of the orthorhombic and trigonal forms with a computer graphics system indicates that the spatial relations among the domains are significantly different. These differences are pronounced in the interactions between homologous domains, in the hapten-binding regions, and in the bends of the V and C domains about the switch regions in both monomer 1 and monomer 2. As a consequence, the "bend" angle defined by the intersection of the two pseudotwofold axes between the V domains and the C domains is larger in the orthorhombic (132°) than in the trigonal form (115°). The orthorhombic form of the light-chain dimer thus resembles antigen-binding (Fab) fragments (comparable bend angles of 130-170°) even more closely than the trigonal form.

Despite a difference in size of ~50000 daltons, the human Zie IgG2 cryoglobulin and the $F(ab')_2$ fragment,[1] prepared from it by peptic hydrolysis, crystallize in the same space group with closely similar unit cell dimensions (Ely et al., 1978b). We concluded that the crystal-packing forces and the overall conformations of the Fab arms were almost identical in the two crystal systems. The human Kol IgG1 protein and its Fab fragment crystallize in different space groups, but the structures of the Fab regions are nearly the same (Colman et al., 1976; Matsushima et al., 1978).

The human Mcg IgG1 euglobulin crystallizes in the same space group in water and in ammonium sulfate, although the b cell edge is about 5% shorter in the latter solvent (Edmundson et al., 1970, and unpublished experiments). In contrast, the Mcg Bence-Jones dimer produces markedly different crystals in water and ammonium sulfate (Edmundson et al., 1971). The Bence-Jones dimer exhibits a wide range of conformational flexibility (Firca et al., 1978; Ely et al., 1978a; Edmundson et al., 1978), and the present study was initiated to determine whether the molecule assumes different conformations in the two solvent systems.

For technical reasons a preliminary investigation of the orthorhombic water form (Schiffer et al., 1970) was deferred in favor of the trigonal ammonium sulfate form (Edmundson et al., 1972, 1975; Schiffer et al., 1973). The early orthorhombic crystals diffracted to 2.3 Å, but they grew as plates, were slow to appear, and were subject to dissolution during storage. The crystals also cracked or dissolved in solutions of heavy-atom derivatives as dilute as 0.001 M. Renewal of the structural study became possible in the past year when one of us (K.R.E.) developed procedures for producing large, relatively stable orthorhombic crystals diffracting to d spacings of <2.0 Å. The improved crystals were used to obtain a low-resolution (6.5-Å) structure by the multiple isomorphous replacement (MIR) method.

Materials and Methods

Preparation of Orthorhombic Crystals. The Mcg Bence-Jones protein was precipitated from urine by the addition of solid ammonium sulfate to 90% saturation. The ammonium sulfate filter paste was dialyzed against distilled water at 4 °C, and ~50% of the protein crystallized overnight. Crystals were harvested by centrifugation, redissolved in 0.02 M sodium phosphate, pH 7.4, and precipitated in 50% saturated ammonium sulfate. The precipitate was isolated by centrifugation and stored at -10 °C. The purity of the protein was checked by $NaDodSO_4$ electrophoresis both in the presence and absence of 2-mercaptoethanol (Laemmli, 1970). Samples used for further crystallization consisted of one principal electrophoretic component representing ~98% of the protein. This component was a dimer (M_r 46000) in which the monomers were covalently linked by an interchain disulfide bond between the penultimate half-cystine residues [see Fett & Deutsch (1974)]. A component present in trace amounts was a dimer held together only by noncovalent forces.

For preparation of crystals for diffraction, the purest samples of covalent dimers were dialyzed at 4 °C and pH 7.4 against 0.02 M Tris-HCl which was 0.001 M in EDTA. The protein was concentrated to 35-40 mg/mL by ultrafiltration. The sample was then dialyzed against deionized water for 6 h and centrifuged to remove precipitate and incipient crystal seeds.

† From the Departments of Biochemistry and Biology, University of Utah, Salt Lake City, Utah 84108. *Received August 16, 1979.* This investigation was supported by Grant No. CA 19616, awarded by the National Cancer Institute, Department of Health, Education, and Welfare.

‡ Present address: Department of Chemistry, Brookhaven National Laboratory, Upton, NY 11973.

[1] Abbreviations used: $F(ab')_2$, peptic fragment of an immunoglobulin, consisting of two antigen-binding arms covalently linked by interchain disulfide bonds; Fab, antigen-binding fragment; MIR, multiple isomorphous replacement; SIR, single isomorphous replacement; $NaDodSO_4$, sodium dodecyl sulfate; EDTA, (ethylenedinitrilo)tetraacetic acid, disodium salt; PCMBS, *p*-(chloromercuri)benzenesulfonic acid; $Pt(CNS)_4^{2-}$, tetrathiocyanoplatinite.

0006-2960/80/0419-0432$01.00/0

Table I: Final Heavy-Atom Parameters and Refinement Statistics

derivative	site	x	y	z	M^a	$R_F{}^b$ (all)	R_F (centric)	$R_C{}^c$ (centric)	$R_K{}^d$ (all)	ERMS[e]
$Pt(CNS)_4{}^{2-}$	1	0.143	0.406	0.672	2.62	0.164	0.219	0.511	0.0078	159.7
PCMBS	1	0.144	0.404	0.687	0.54	0.130	0.159	0.535	0.0068	150.0
	2	0.112	0.071	0.182	1.84					
	3	0.341	0.226	0.119	1.27					
ethyl-Hg-PO_4 (I)[f]	1	0.157	0.405	0.697	1.13	0.113	0.144	0.538	0.0056	130.8
	2	0.085	0.082	0.171	0.80					
	3	0.385	0.207	0.115	1.18					
	4	0.128	0.081	−0.219	0.30					
	5	0.334	0.180	0.596	0.19					
	6	0.199	0.387	0.088	0.24					
	7	0.043	0.399	0.252	0.22					
ethyl-Hg-PO_4 (II)	1	0.155	0.405	0.693	1.12	0.104	0.132	0.565	0.0053	111.7
	2	0.083	0.079	0.171	0.72					
	3	0.382	0.207	0.115	1.01					

[a] Occupancies on a relative scale. The isotropic temperature factors (B) were set at 7 Å^2 and were not refined. The scattering form factor for mercury was used for all derivatives. [b] $R_F = \Sigma|F_{PH} - F_P|/\Sigma|F_P|$, where F_{PH} and F_P are the observed structure amplitudes of the derivatives and native protein. [c] $R_C = \Sigma|F_{H,o} - \bar{F}_{H,c}|/\Sigma|F_{H,o}|$, where $F_{H,o}$ and $F_{H,c}$ are the observed and calculated structure amplitudes of the heavy atom (centric). [d] $R_K = \Sigma|F_{PH,o} - F_{PH,c}|/\Sigma|F_{PH,o}|$. [e] ERMS = root mean square estimate of error for each derivative. The values for ERMS/$\bar{F}_H$ are 0.431, 0.457, 0.482, and 0.471 for the derivatives. $\bar{F}_H$ is the calculated average structure amplitude for the heavy-atom contributions in each derivative. The mean residual error (Dickerson et al., 1968) is 3.6, and the figure of merit is 0.88 (all; 0.96, centric). [f] The volume of crystal I was only two-thirds as large as that of crystal II. The volume and concentrations of ethylmercuric phosphate, as well as other soaking conditions, were the same in the two crystals.

The supernate was transferred to microdiffusion tubes (Zeppezauer et al., 1968) and dialyzed against deionized water in an incubator in which the temperature was controlled at 15 ± 2 °C. Prismatic crystals that appeared in 2–4 weeks were elongated along the b axis and were 0.5–0.7 mm in the shortest dimension. Only 4–5 crystals of such size were obtained from 100 mg of protein. In the absence of the precautions listed above, the protein produced showers of unusable small crystals.

The large crystals gave the same diffraction patterns as the crystals used in the preliminary study (Schiffer et al., 1970). The orthorhombic space group was $P2_12_12$, with a = 72.6, b = 81.9, and c = 71.0 Å. The crystallographic asymmetric unit was the covalently linked dimer. The partial volume of solvent calculated for the earlier crystals was 0.46, a value consistent with solvent distribution in the electron density map for the present crystals.

Preparation of Heavy-Atom Derivatives. The present crystals were able to tolerate most heavy-atom salts in concentrations of 0.6 mM. In a typical experiment a crystal in 30 μL of mother liquor was drawn into a capillary of the type used for collection of diffraction data. A 3-μL aliquot of a 6 mM solution of heavy-atom derivative in 0.3 mM buffer (usually sodium phosphate, pH 6.2) was added to the mother liquor. The capillary was sealed with dental wax and stored at 4 °C for periods of 1–4 weeks (or until incipient cracking of the crystal was observed).[2] The liquid was removed, and the crystal was aligned with the b axis parallel to the length of the capillary. Reservoirs of deionized water were placed near the crystal before the capillary was sealed to compensate for the tendency of these crystals to dry out when exposed to the X-ray beam. Reservoirs of mother liquor and/or heavy-atom solutions were less effective for this purpose.

[2] We do not wish to gloss over the difficulties of preparing derivatives in crystals with mother liquor of such low ionic strength. Crystals from different preparations and individual crystals from one preparation vary in their resistance to cracking or dissolution in heavy-atom solutions. The use of small volumes (e.g., 33 μL) to minimize these difficulties can lead to different occupancies in successive soaking experiments or to different patterns of substitutions in minor sites. For example, compare the heavy-atom parameters in Table I for the ethylmercuric phosphate derivatives I and II, in which crystals of unequal size were treated with the same quantity of heavy-atom solution for the same period of time.

Heavy-atom compounds initially selected for trials were those applied to the solution of the dimeric structure in trigonal crystals: namely, the organic mercurials *o*-(chloromercuri)-phenol, *p*-(hydroxymercuri)benzenesulfonic acid, merthiolate, mercuhydrin, mersalylsodium, phenylmercuric salts, and methylmercuric chloride. Surprisingly, these compounds either cracked the crystals or did not cause sufficient changes in reflection intensities to be considered derivatives. A derivative with a mercury atom covalently inserted between the sulfur atoms of the interchain disulfide bond (Ely et al., 1973) has been crystallized in the orthorhombic form, but the crystals are as yet too small for diffraction experiments.

Compounds which did form usable derivatives included *p*-(chloromercuri)benzenesulfonic acid (PCMBS), tetrathiocyanoplatinite [$Pt(CNS)_4{}^{2-}$], and ethylmercuric phosphate. The ethylmercuric phosphate was kindly provided by Dr. G. Petsko.

Collection of Diffraction Data. In contrast to the Mcg trigonal form of the Bence–Jones dimer and the IgG1 immunoglobulin, which have 186-Å unit cell axes (Edmundson et al., 1971), the orthorhombic form poses no special problems in resolution of closely spaced reflections (the longest axis is 82 Å long). The Syntex $P2_1$ diffractometer, which was assembled with a crystal to detector distance of 62 cm to accommodate the trigonal and IgG1 proteins, was not altered to collect data for the orthorhombic crystals.

Data for crystals of native protein were collected in shells to 2.0-Å resolution. When drying of the crystal in the capillary was minimal and the temperature of the room was maintained at 13 ± 1 °C, data were generally collected for 50–60 h with Cu Kα radiation at 40 kV, 20 mA. During this period the average decrease in intensities of three check reflections was 20–25% in the 15–25° range of 2θ. Above ambient temperatures of 23 °C the crystals tended to dissolve in the X-ray beam in ~30 h. Under ideal conditions and in exceptional cases, crystals of the native protein have yielded useful data for periods up to 150 h. In the 6.5-Å shell (2θ = 13.7°) for which the present structure is reported, there were 973 reflections with 886 observed at the 3σ level.

Most of the large crystals were used to collect the set of native data, and the heavy-atom screening process was initially limited to a 6.5-Å search. The stocks of crystals are currently

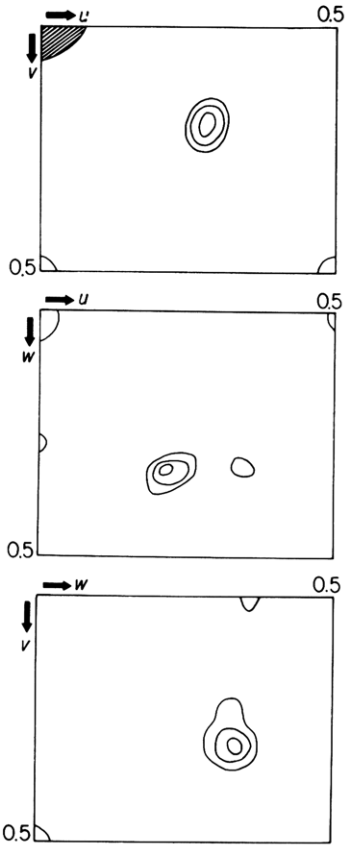

FIGURE 1: Difference Patterson–Harker sections for the $Pt(CNS)_4^{2-}$ derivative. The contours are at equal arbitrary intervals above zero, with the height of the origin peak being 1000. The three Harker peaks represent site 1 in Table I.

being replenished to extend the results to higher resolution.

Determination of Heavy-Atom Positions. Three-dimensional difference Patterson functions[3] were initially computed for the $Pt(CNS)_4^{2-}$ and PCMBS derivatives. The Harker sections for the $Pt(CNS)_4^{2-}$ derivative are shown in Figure 1. The vectors clearly indicate the location of a single site (no. 1 in Table I). By use of this site and all of the data, five cycles of single isomorphous replacement (SIR) refinement were performed by the method of least squares (Dickerson et al., 1968). The phase angles generated in the refinement procedure were used to prepare an unweighted $2F_o - F_c$ map with coefficients $2F_{PH,o} - F_{PH,c}$ and phases $\alpha_{PH,c}$. This map is a variation of the "residual" map suggested by Matthews (1970). It has the advantage that major and minor heavy-atom sites appear with peak heights proportional to their occupancies (J. E. Abola, personal communication).

In the case of the PCMBS derivative, a prominent site (no. 2 in Table I) was easily located by inspection of the three Harker sections. After five cycles of SIR refinement, a $2F_o - F_c$ map was prepared and sites 1 and 3 in Table I were identified by inspection. The existence of minor site 1 was confirmed by another cycle of refinement and calculation of a $2F_o - F_c$ map. When the difference Patterson map was reexamined, it was found that the 10 highest peaks (excluding the origin) could be explained by the Harker vectors for the major site and the vectors between the major and minor sites.

By use of the protein phases determined with $Pt(CNS)_4^{2-}$, a three-dimensional difference Fourier map was calculated for the PCMBS derivative. The map showed all three substitution sites for the latter derivative. The refinement results were also used to compute a $2F_o - F_c$ map, which revealed the three PCMBS sites with the expected occupancy ratios.

The locations of the substitution sites in the two ethylmercuric phosphate derivatives (see Table I) were determined by difference Fourier analysis, using the phases from the SIR refinement of the $Pt(CNS)_4^{2-}$ derivative.

The coordinates and occupancies of the heavy atoms of all four derivatives were then refined together, with alternating cycles of phase angle determinations and least-squares refinement (Dickerson et al., 1968). Initially, only centric data were included to obtain approximate occupancy values. The isotropic temperature factor (B) was held constant at 7 Å^2. The refinement converged rapidly, and the statistics were very encouraging. The heavy-atom parameters and summary statistics for the refinement are presented in Table I.

[3] The coefficients were of the form $|\Delta F|^2 = (|F|_{PH} - |F|_P)^2$, where $|F|_{PH}$ and $|F|_P$ are the observed structure amplitudes of the derivative and the native protein.

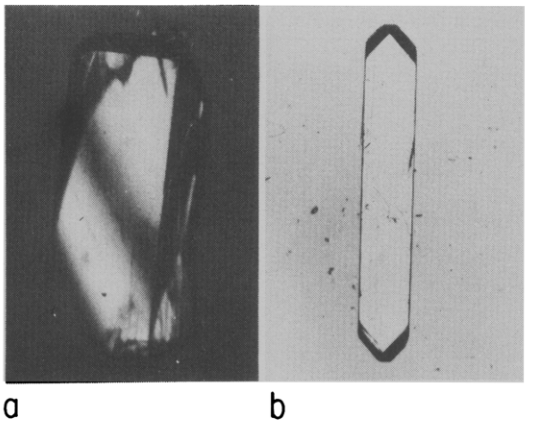

FIGURE 2: Photographs of new (a) and old (b) versions of orthorhombic crystals produced by dialysis of the Mcg Bence–Jones dimer against deionized water. Note that the new type is much wider and thicker relative to its length. In both cases the space group is $P2_12_12$, with $a = 72.6$, $b = 81.9$, and $c = 71.0$ Å. The solvent content in each crystal is estimated to be 46%, and the crystallographic asymmetric unit is the dimer (M_r 46 000). The principal difference in the procedures for preparing the crystals is attention to detail. Protein samples used for the new type are selected from our most homogeneous stocks (electrophoretically estimated to be >98% covalently linked dimers). After preliminary treatment with EDTA and initiation of crystallization by dialysis against deionized water, small seeds and amorphous precipitates are removed by centrifugation. Large crystals appear as the dialysis of the supernate is continued.

Results and Discussion

Crystals of the Orthorhombic Form. Photographs of the old and new orthorhombic crystals are shown in Figure 2. Note that the new crystals are wider and thicker than the old. Both old and new types can readily be cut into shapes appropriate for diffraction by cleavage along planes perpendicular to the long axes (b) of the crystals. Two and occasionally three usable fragments can be obtained from one crystal. Twinning is common, but the crystals are mechanically stable and satellites can be carved away from the faces.

The solubility of the Bence–Jones dimer contrasts sharply with the Mcg IgG1 protein, a euglobulin which precipitates or crystallizes to the extent of 90% when dialyzed against water overnight at 4 °C [H. F. Deutsch, as quoted in Edmundson et al. (1970)]. Orthorhombic crystals of the Bence–Jones dimer can also be produced rapidly by dialysis against water at 4 °C, but ~50% of the protein remains in the supernate. Perturbations such as additions of salt to greater than millimolar concentrations and temperature increases, particularly in the presence of the X-ray beam, encourage shifts from

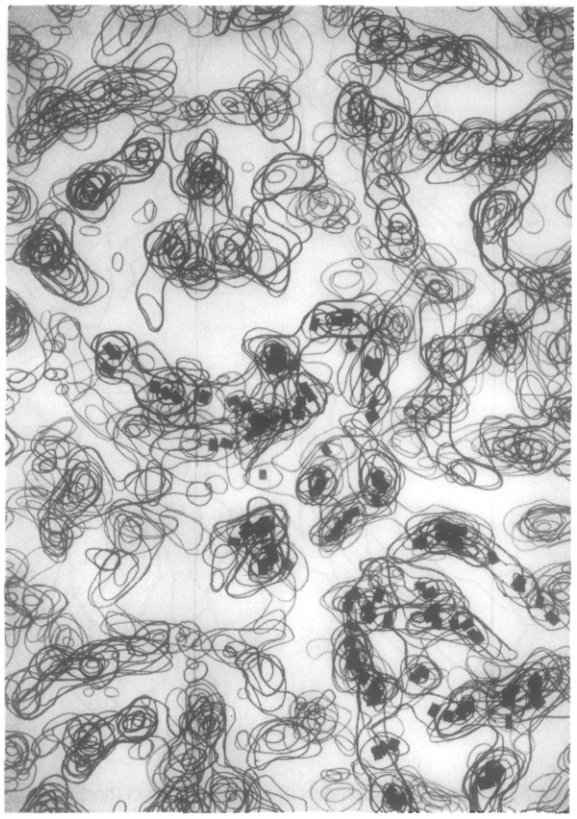

FIGURE 3: Superposed sections of part of the 6.5-Å electron density map for the orthorhombic form of the Mcg Bence–Jones dimer. Sections are normal to the a axis, from $x = -0.2$ to $+0.08$, with y the ordinate and z the abscissa in each section. The map is plotted on an arbitrary scale, and the maximum value is set at 1000. Contours are at equal intervals of 200, with zero contours omitted. Modules of electron density corresponding to the asymmetric unit are marked with pieces of tape (only part of the molecule is shown in these sections). Models of domains based on the high-resolution structure of the trigonal form of the Bence–Jones dimer (Edmundson et al., 1975) were fitted into this map. This fitting procedure indicated clearly that the module in the lower right-hand corner represents the dimer of C domains. A symmetry-related C domain module is found at the lower left-hand corner. The sets of density for the two C modules are repeated in the upper corners of the map (i.e., are related by unit cell translations). The contours in the middle of the map correspond to part of the V domain dimeric module.

crystalline to liquid states. The heavy-atom compounds listed in Table I apparently have sufficient affinity for targeted sites to form derivatives at low concentrations, without changes of state or overt destruction of the crystal lattice.

General Locations of Heavy-Atom Substitution Sites. Since there were only three major substitution sites, it was relatively straightforward to assign their general locations with the aid of the atomic model of the trigonal form and the complete amino acid sequence of the molecule (Fett & Deutsch, 1974). As emphasized in the next section, the high quality of the electron density map of the orthorhombic form allowed us to fit models with confidence.

Site 1 in Table I appears to be located in the vicinity of histidine-192 of the C domain of monomer 2. It is not clear why the comparable site in the C domain of monomer 1 is not occupied. Sites 2 and 3 correspond to the surface crevices centered about the histidine-41 residues in the V domains (site 2 is in monomer 1 and site 3 is in monomer 2). The results indicate that PCMBS acts primarily as a V domain marker, with preferential binding to monomer 1. $Pt(CNS)_4^{2-}$ is a C domain marker and specific for monomer 2. Ethylmercuric phosphate lodges in all three major sites in the V and C domains and in several minor sites.

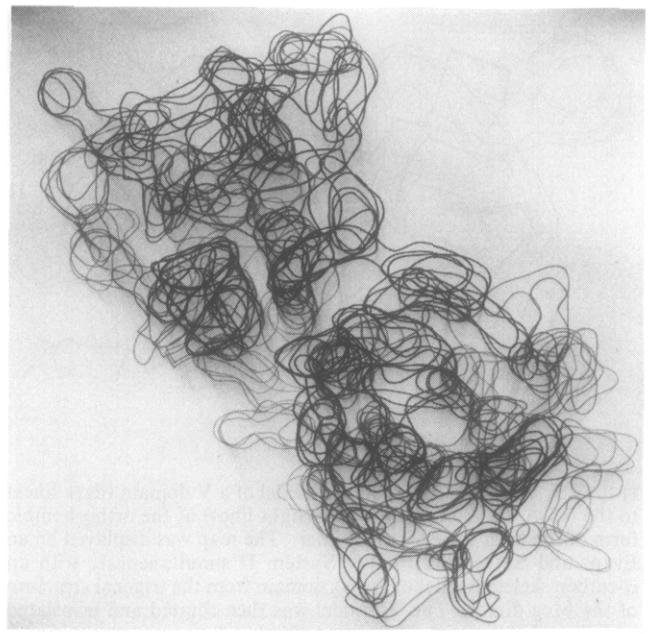

FIGURE 4: Photograph of superposed sections of electron density representing the Mcg Bence–Jones dimer. The 200 level contours [$\sim 1\sigma(\rho)$] assigned to the asymmetric unit as in Figure 3 were isolated and traced onto sheets of Plexiglas. The modules of electron density are in the same orientation as those in Figure 3. The V dimeric module is on the upper left, and the C dimeric module is on the lower right.

It is of interest to compare the substitution sites in the trigonal and orthorhombic forms, with a view toward explaining the surprising failures of the trigonal series of compounds to form derivatives in orthorhombic crystals. In the trigonal form, *o*-(chloromercuri)phenol, *p*-(hydroxymercuri)benzenesulfonate, and methylmercuric chloride were found in the histidine-41 crevices of monomers 1 and 2 with approximately equal occupancies (Schiffer et al., 1973). The region around histidine-192 was only a secondary site. The conical main cavity for the binding of haptenlike molecules between the two V domains at the tip of the dimer contains two subsites, A and B (Edmundson et al., 1974). Among the heavy-atom compounds binding in these subsites in the trigonal form are the mercurials merthiolate, mersalyl, and mercuhydrin. Phenylmercuric compounds and *o*-(chloromercuri)-phenol lodge in the deep pocket (site C) continuing from the base of the main cavity. These compounds have not been detected in corresponding locations in the orthorhombic crystals. At low resolution the access routes to the sites appear to be more congested in the crystal lattice of the orthorhombic form.

The differences in the patterns of substitutions in the two crystal systems are less difficult to understand in the context of the substantial structural differences to be discussed in the following sections.

Electron Density Maps. By use of "best" phase angles (Blow & Crick, 1959), electron density maps were calculated at 6.5-Å resolution in planes perpendicular to the a axis. Contours were drawn on an arbitrary scale at intervals of 200 [$\sim 1\sigma(\rho)$] from 0 to 1000, with the zero contours omitted. A representative set of stacked Plexiglas sheets of the map is shown in Figure 3. In lieu of the usual balsa wood model to show the general shape of the molecule, the contours corresponding to the dimer were isolated and redrawn to give Figure 4.

The molecular boundaries of the dimer are well-defined in Figure 3, although the solvent channels are less prominent than

FIGURE 5: Fitting of a wire frame model of a V domain (dark lines) to the 6.5-Å electron density map (light lines) of the orthorhombic form of the Mcg Bence–Jones dimer. The map was displayed on an Evans and Sutherland Picture System II simultaneously with an α-carbon skeletal model of the V_2 domain from the trigonal structure of the Mcg dimer. The V_2 model was then rotated and translated with the aid of "joysticks" until an optimal fit to the map was achieved.

in the map for trigonal crystals (Edmundson et al., 1972). The characteristic modules of electron density, representing either the V_1–V_2 domain pair or the C_1–C_2 dimer, are clearly distinguishable in the map. Parts of more than one unit cell are included in Figure 3, and the V_1–V_2 dimeric module in the middle of the figure is surrounded by C_1–C_2 modules at the four corners.

Without prior knowledge of the structure, it was possible to connect the V_1–V_2 module to the C_1–C_2 module in more than one way at this resolution. The map was therefore computed on the same scale (2.5 Å/cm) as αC wire models ("Byron's Bender"; Charles Supper Co.) of the Mcg V and C domains found in the trigonal form. The models were fitted into the map with the aid of an optical comparator (Richards, 1968). With this procedure the V and C modules could be linked unequivocally and all electron density in the map could be assigned to one or the other type of module. The assignments were consistent with the strict symmetry requirements of the space group $P2_12_12$; i.e., a dimer cannot cross the crystallographic twofold axes of rotation parallel to z at x = 0 and $^1/_2$ and y = 0 and $^1/_2$. In the unit cell there are four dimers, each of which is approximately the same length ($\sim$75 Å) as the a (72.3 Å) and c (71.0 Å) cell edges. With such tight packing, it is not surprising that the partial solvent volume is low (0.46) relative to that (0.60) in trigonal crystals (Edmundson et al., 1971).

The fitting of αC models to electron density of the orthorhombic form was convincing only when individual V or C domains were used. Models of V and C domains mechanically connected to simulate intact monomers 1 and 2 in the trigonal structure could not be made to fit the density. Two approaches were taken to provide an explanation for this finding.

(1) The density corresponding to an orthorhombic asymmetric unit was isolated, replotted on Plexiglas sheets, and compared with a 6.5-Å electron density map for the dimer in the trigonal crystal system. The spatial relations between the V and C dimeric modules were quite different in the two maps.

(2) With a set of protein modeling programs written by Dr. Russell Athay, electron density contours for the orthorhombic asymmetric unit were selected from the 6.5-Å map and displayed on an Evans and Sutherland Picture System II, interfaced to a DEC PDP 11/70 computer. The programs permitted interactive three-dimensional fitting of αC skeletal models of the V and C domains into the density (with the aid of "joysticks" for rotations and translations). The interactive system allows the operator to manipulate the backbone of each domain as a rigid unit and to examine the fit from any view or orientation.

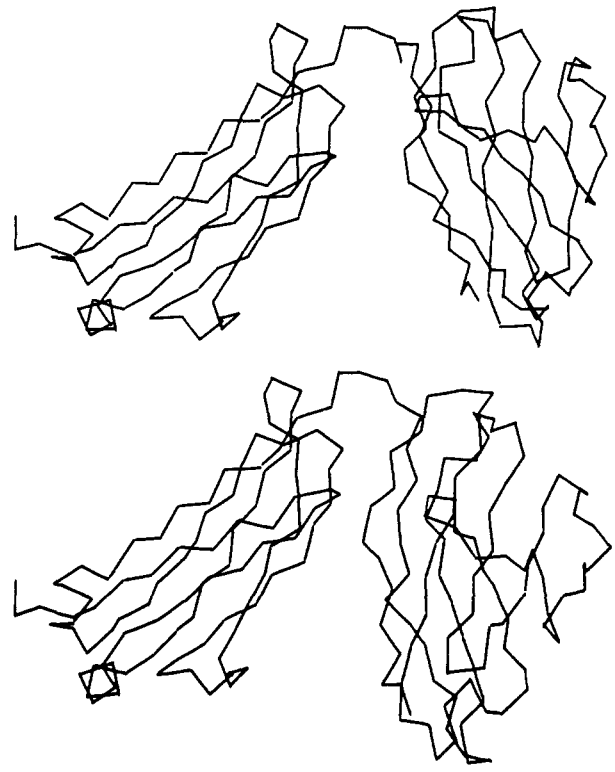

FIGURE 6: Comparison of models of monomer 1 in orthorhombic (top) and trigonal (bottom) forms. Models of V_1 and C_1 domains were fitted independently to the 6.5-Å electron density map with the aid of our computer graphics system (see Figure 5). The V_1 and C_1 domains in their new orientations were displayed simultaneously to produce a facsimile of monomer 1. The V_1 domain is on the upper right, and the C_1 domain is on the upper left. The carboxyl end of the V domain closely approaches the amino end of the C domain in the space between the two domains (i.e., in the switch region). The juxtaposition of the chain ends gives us confidence in the procedure for independently fitting domains to the electron density. For a comparison of monomer 1 in the orthorhombic form with that of the trigonal form, the two structures were displayed simultaneously and the C domains were placed in approximately the same orientations. In particular, note the wider separation of the V and C domains in the orthorhombic form and the substantial differences in the orientations of the V domains.

An example of the fitting process for the V domain is shown in Figure 5.

After each domain was fitted separately, the resulting models of the V and C domains of each monomer were displayed simultaneously to see if the carboxyl end of the V domain could form a proper connection with the amino end of the C domain. These tests for connectivity in the switch regions were highly successful and gave us confidence in the accuracy of the assignments. Photographs of the models of orthorhombic monomers 1 and 2 are presented in Figures 6 and 7, with the corresponding trigonal models shown for comparison.

As a further check on the fitting procedure, the models of the V_1, V_2, C_1, and C_2 domains were displayed simultaneously to see if they formed a plausible dimer. In the resulting composite structure (see Figure 8), the domains were found in positions favorable for stabilization of dimeric modules without any demonstrable steric interference along the interacting surfaces.

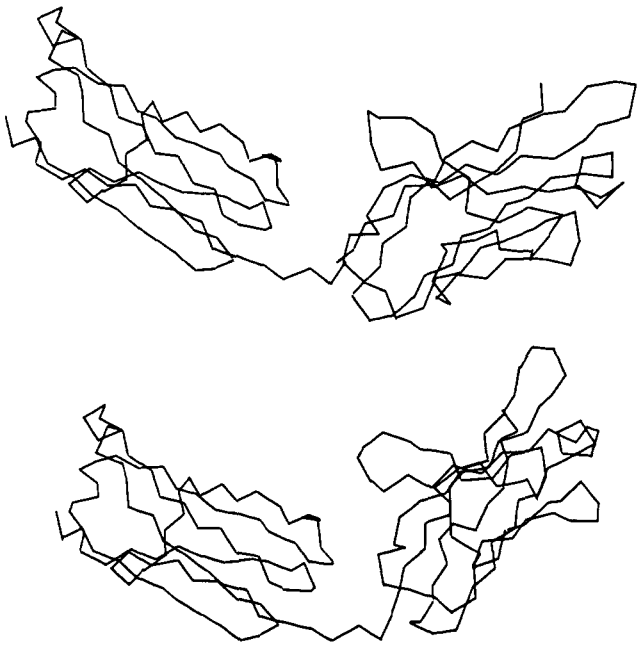

FIGURE 7: Comparison of models of monomer 2 in orthorhombic (top) and trigonal (bottom) forms. Individual V_2 (right) and C_2 (left) domains were fitted into the electron density map as in Figure 6. The C domains of the orthorhombic and trigonal forms are placed in the same orientations. Note that monomer 2 in the orthorhombic form is more extended. In addition, the torsional relationship between the V and C domains is significantly different, as are the spatial relations among the loops projecting into the space between the V and C domains.

Major Differences in the Structures of the Orthorhombic and Trigonal Forms of the Bence–Jones Dimer. Even at low resolution it is clear that the Bence–Jones protein has assumed significantly different conformations in the two crystal systems.

Both monomers show major differences from the trigonal chains. The orthorhombic form of monomer 1 has a less acute "elbow bend" around the switch region and substantially different spatial relations between the V and C domains (see Figure 6). The V–C interactions were particularly prominent in the 6-Å map of the trigonal form, appearing as two bands of continuous density bridging the V and C domains (Edmundson et al., 1972). These interactions were later found to involve mainly two pairs of residues, proline-7 (V) in contact with valine-147 (C) and serine-9 (V) within hydrogen-bonding distance of glutamic acid-202 (C) (Schiffer et al., 1973; Edmundson et al., 1975). In the orthorhombic form, the V–C interactions of monomer 1 appear to be less pronounced.

Monomer 2 is also more extended than its trigonal counterpart, and the torsional relation between V and C domains is noticeably different (Figure 7). There are no V–C contacts in monomer 2 in the trigonal structure, and the opposing loops along the V–C boundaries seem to have rolled even farther away in the orthorhombic form.

Pseudotwofold Axes of Rotation in the Orthorhombic Form of the Bence–Jones Dimer. Inspection of the model of the orthorhombic structure indicated that pairs of domains (V_1–V_2 and C_1–C_2) were probably related by pseudotwofold axes of rotation similar to those observed in the trigonal form. The model of the orthorhombic dimer obtained with the graphics system was used to generate a set of αC coordinates. The approximate positions of the pseudodiads were determined with this set of coordinates, using a least-squares fitting procedure (Huber et al., 1971; the program ROTMOL and instructions for its use were kindly supplied by Drs. W. Steigemann, P. Colman, and R. Huber). The pseudodiads are superimposed on the model of the dimer depicted in Figure 8.

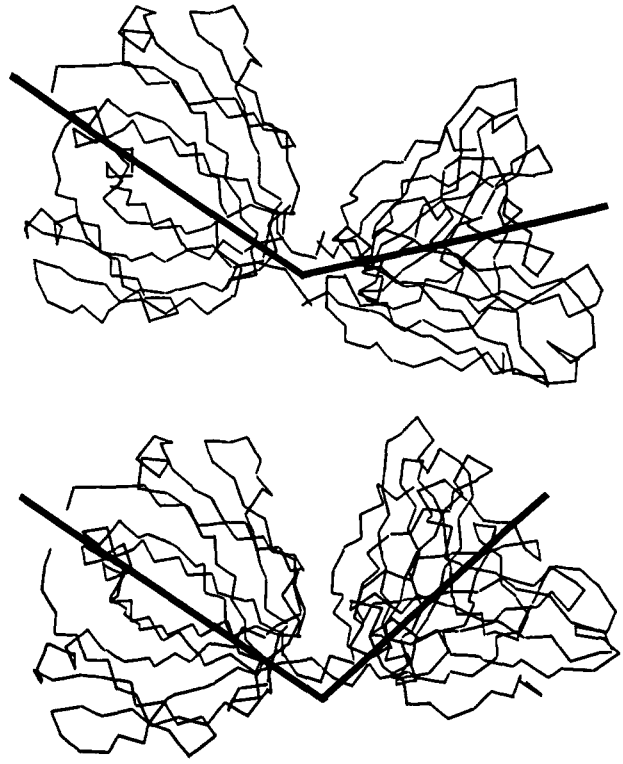

FIGURE 8: Comparison of models of the Mcg Bence–Jones dimer in orthorhombic (top) and trigonal (bottom) forms. Models of the V_1, V_2, C_1, and C_2 domains, all fitted independently to the electron density, were displayed simultaneously on the Picture System. Without alteration, the four domains formed a dimer in which there was no demonstrable steric interference along the interacting surfaces. For comparison of the orthorhombic and trigonal forms, the two structures were displayed and the C_1 domains (upper left in each dimer) were placed in the same orientations. With such different monomeric structures in the two forms, it is not surprising that the dimers also look different. The pseudotwofold axes of rotation between pairs of homologous domains are superimposed on the models of the dimers. The V_1–V_2 and C_1–C_2 pseudodiads intersect at angles of 132° in the orthorhombic form and 115° in the trigonal form.

The angle subtended by the intersection of the two pseudodiads was 132° (see Figure 8), a value significantly higher than the corresponding angle (115°) obtained for the trigonal form by the same procedure. The difference in these angles reflects the marked structural differences in the dimers, as displayed in Figure 8.

Similar angles of 130–136° have been reported for human and murine Fab fragments (Poljak et al., 1974, 1976; Segal et al., 1974; Davies et al., 1975; Padlan et al., 1976). In the case of the Kol Fab fragment, however, the angle is 166° (Matsushima et al., 1978). The Fab angles in the intact Mcg, Dob, and Kol IgG1 immunoglobulins are 128°, 147°, and 174°, respectively (Panagiotopoulos et al., 1977; Silverton et al., 1977; Colman et al., 1976). In regard to these angles and their structural implications, the orthorhombic form of the Mcg Bence–Jones dimer resembles Fab regions even more closely than the trigonal form.

Although differing in detail, the structural elements interacting in the zones surrounding the pseudodiads in the V dimeric modules are similar in the Mcg Bence–Jones dimer and Fab fragments, as well as in dimers of V domains of light chains. Examples of such V_L dimers are the Au and Rei κ-type molecules, the domains of which are related by a crystallographic diad and a pseudodiad, respectively (Fehlhammer et al., 1975; Epp et al., 1974, 1975). In the Rhe λ-type V_L dimer, however, the interactions between V domains and the geometry

of the interdomain cavity are different from those in the Rei and Au dimers and by implication the Mcg Bence–Jones protein and Fab fragments (Wang et al., 1979).

Concluding Remarks. The magnitude of the structural differences in the trigonal and orthorhombic forms caught us by surprise. We inadvertently had demonstrated 10 years ago that these structures are interchangeable. The protein samples used to prepare all trigonal crystals for X-ray analysis were obtained by dissolving orthorhombic crystals (when the protein was fresh, the easiest method of purification was crystallization by dialysis against water).

The structural transitions of the dimer in ammonium sulfate and water occur in the presence of an intact interchain disulfide bond. When conformational changes are induced in the dimer by the binding of haptenlike molecules [e.g., bis(dinitrophenyl)lysine], the interchain disulfide bond locks the protein in a stable, but abnormal form which only crystallizes as needles in ammonium sulfate (Firca et al., 1978; Ely et al., 1978a). These changes can be reversed by cleavage and slow reoxidation of the interchain disulfide bond, whereupon the normal trigonal crystal form is produced in ammonium sulfate [for recent solution studies on the effect of the interchain disulfide bond on the hapten-binding properties of the MOPC-315 light-chain dimer, see Zidovetzki et al. (1979)].

The Mcg light chain behaves as yet another conformational isomer when associated with the heavy chain in the IgG1 immunoglobulin. After reversible cleavage of the interchain disulfide bond, the light chains can be dissociated from the heavy chains and reassembled into a dimer indistinguishable from the native Bence–Jones dimer in its trigonal form (Firca et al., 1978; Ely et al., 1978a). Conversely, monomers 1 and 2 of the Bence–Jones dimer can be converted to the single conformational isomer associated with the heavy chain in the IgG1 protein.

In sum, the Mcg light chain has been identified in five crystallographically distinct native conformations, two in the trigonal form, two in the orthorhombic form, and one in the IgG1 molecule, as well as one and probably more abnormal conformations in needle forms. Conformational flexibility thus appears to be a key property in the ability of the light-chain monomer to adapt to whatever conditions are necessary for its function and in the ability of the light-chain dimer to mimic an Fab fragment.

The patient Mcg died of complications associated with amyloidosis, in which intact or degraded light chains were assumed to be important constituents of the amyloid deposits (Deutsch, 1971; Osserman, 1976). To correlate our structural results with chemical and medical observations on amyloid fibrils, we have continued to look for crystals grown under more physiological conditions than the trigonal forms produced in ammonium sulfate. In the orthorhombic form, we seem to have an excellent model system for exploring the structural changes involved in the conversion of flexible, globular molecules into deleterious, insoluble fibrils.

Acknowledgments

We thank Dr. Russell J. Athay for developing and implementing a protein modeling system for use with our Evans and Sutherland Picture System II. Drs. S. Swanson and E. F. Meyer, Jr., kindly supplied their contouring programs which were integrated into our protein modeling system. Drs. R. Diamond and G. Cohen sent us a DEC 11/70 version of the BILDER graphics system and offered many helpful suggestions to strengthen our programs. We are deeply grateful to Robin Wilk for her repeated efforts to provide us with enough crystals to carry out this work.

References

Blow, D. M., & Crick, F. H. C. (1959) *Acta Crystallogr. 12*, 794.

Colman, P. M., Deisenhofer, J., Huber, R., & Palm, W. (1976) *J. Mol. Biol. 100*, 257.

Davies, D. R., Padlan, E. A., & Segal, D. M. (1975) *Annu. Rev. Biochem. 44*, 639.

Deutsch, H. F. (1971) *Seibutsu Butsuri Kagaku 16*, 73.

Dickerson, R. E., Weinzierl, J. E., & Palmer, R. A. (1968) *Acta Crystallogr., Sect. B 24*, 997.

Edmundson, A. B., Wood, M. K., Schiffer, M., Hardman, K. D., Ainsworth, C. F., Ely, K. R., & Deutsch, H. F. (1970) *J. Biol. Chem. 245*, 2763.

Edmundson, A. B., Schiffer, M. K., Wood, M. K., Hardman, K. D., Ely, K. R., & Ainsworth, C. F. (1971) *Cold Spring Harbor Symp. Quant. Biol. 36*, 427.

Edmundson, A. B., Schiffer, M., Ely, K. R., & Wood, M. K. (1972) *Biochemistry 11*, 1822.

Edmundson, A. B., Ely, K. R., Girling, R. L., Abola, E. E., Schiffer, M., Westholm, F. A., Fausch, M. D., & Deutsch, H. F. (1974) *Biochemistry 13*, 3816.

Edmundson, A. B., Ely, K. R., Abola, E. E., Schiffer, M., & Panagiotopoulos, N. (1975) *Biochemistry 14*, 3953.

Edmundson, A. B., Ely, K. R., & Abola, E. E. (1978) *Contemp. Top. Mol. Biol. 7*, 95.

Ely, K. R., Girling, R. L., Schiffer, M., Cunningham, D. E., & Edmundson, A. B. (1973) *Biochemistry 12*, 4233.

Ely, K. R., Firca, J. R., Williams, K. J., Abola, E. E., Fenton, J. M., Schiffer, M., Panagiotopoulos, N. C., & Edmundson, A. B. (1978a) *Biochemistry 17*, 158.

Ely, K. R., Colman, P. M., Abola, E. E., Hess, A. C., Peabody, D. S., Parr, D. M., Connell, G. E., Laschinger, C. A., & Edmundson, A. B. (1978b) *Biochemistry 17*, 820.

Epp, O., Colman, P., Fehlhammer, H., Bode, W., Schiffer, M., Huber, R., & Palm, W. (1974) *Eur. J. Biochem. 45*, 513.

Epp, O., Lattman, E. E., Schiffer, M., Huber, R., & Palm, W. (1975) *Biochemistry 14*, 4943.

Fehlhammer, H., Schiffer, M., Epp, O., Colman, P. M., Lattman, E. E., Schwager, P., Steigemann, W., & Schramm, H. J. (1975) *Biophys. Struct. Mech. 1*, 139.

Fett, J. W., & Deutsch, H. F. (1974) *Biochemistry 13*, 4102.

Firca, J. R., Ely, K. R., Kremser, P., Westholm, F. A., Dorrington, K. J., & Edmundson, A. B. (1978) *Biochemistry 17*, 148.

Huber, R., Epp, O., Steigemann, W., & Formanek, H. (1971) *Eur. J. Biochem. 19*, 42.

Laemmli, U. K. (1970) *Nature (London) 227*, 680.

Matsushima, M., Marquart, M., Jones, T. A., Colman, P. M., Bartels, K., Huber, R., & Palm, W. (1978) *J. Mol. Biol. 121*, 441.

Matthews, B. W. (1970) in *Crystallographic Computing* (Ahmed, F. R., Ed.) p 146, Munksgaard, Copenhagen.

Osserman, E. F. (1976) in *Amyloidosis* (Wegelius, O., & Pasternack, A., Eds.) p 223, Academic Press, New York.

Padlan, E. A., Davies, D. R., Rudikoff, S., & Potter, M. (1976) *Immunochemistry 13*, 945.

Panagiotopoulos, N. C., Abola, E. E., Ely, K. R., Schiffer, M., & Edmundson, A. B. (1977) *Am. Cryst. Assoc. Meet., Asilomar, EA 1*, 16.

Poljak, R. J., Amzel, L. M., Chen, B. L., Phizackerley, R. P., & Saul, F. (1974) *Proc. Natl. Acad. Sci. U.S.A. 71*, 3440.

Poljak, R. J., Amzel, L. M., & Phizackerley, R. P. (1976) *Prog. Biophys. Mol. Biol. 31*, 67.

Richards, F. M. (1968) *J. Mol. Biol. 37*, 225.

Schiffer, M., Hardman, K. D., Wood, M. K., Edmundson, A. B., Hook, M. E., Ely, K. R., & Deutsch, H. F. (1970) *J. Biol. Chem. 245*, 728.
Schiffer, M., Girling, R. L., Ely, K. R., & Edmundson, A. B. (1973) *Biochemistry 12*, 4620.
Segal, D. M., Padlan, E. A., Cohen, G. H., Rudikoff, S., Potter, M., & Davies, D. R. (1974) *Proc. Natl. Acad. Sci. U.S.A. 71*, 4298.
Silverton, E. W., Navia, M. A., & Davies, D. R. (1977) *Proc. Natl. Acad. Sci. U.S.A. 74*, 5140.
Wang, B.-C., Yoo, C. S., & Sax, M. (1979) *J. Mol. Biol. 129*, 657.
Zeppezauer, M., Ecklund, H., & Zeppezauer, E. S. (1968) *Arch. Biochem. Biophys. 126*, 564.
Zidovetzki, R., Licht, A., & Pecht, I. (1979) *Proc. Natl. Acad. Sci. U.S.A.* (in press).

Mechanism of the Spontaneous Transfer of Phospholipids between Bilayers†

M. A. Roseman‡ and T. E. Thompson*

ABSTRACT: A fluorescent phospholipid, 1-palmitoyl-2-pyrenedecanoylphosphatidylcholine, was used to study the mechanism of spontaneous phospholipid transfer between single-walled phospholipid vesicles. The half-time for transfer of this molecule between vesicles of dimyristoylphosphatidylcholine at 36 °C is 13 h if flip-flop is negligible or 24 h if flip-flop is faster than intervesicle exchange. The half-time is unaffected by the concentration of acceptor vesicles, which indicates that transfer of label takes place by diffusion of monomers or micelles through the aqueous phase rather than by collision of vesicles. These results are compared with previous studies of spontaneous lipid transfer.

Recent studies have shown that phospholipids spontaneously transfer between phospholipid vesicles with half-times that range from 2 to 24 h, depending on the particular lipid and temperature (Martin & MacDonald, 1976; Duckwitz-Peterlein et al., 1977; Kremer et al., 1977; Papahadjopoulos et al., 1976).[1] In contrast to the obligatory one-for-one exchange reaction catalyzed by phospholipid exchange proteins (Wirtz, 1974), spontaneous flux usually leads to a net transfer of lipid from one membrane to another. This process, if it occurs in vivo, may in part determine the composition of biological membranes.

The purpose of the present study is to determine the mechanism of spontaneous phospholipid transfer. Presumably, there are only two simple mechanisms, which are kinetically distinguishable: either (1) lipid transfers as monomers or micelles through the aqueous phase or (2) lipid transfers upon collision of the membranes. In the studies cited above, calorimetric or light-scattering techniques were used to measure the transfer of phospholipids between liposomes or unilamellar vesicles composed of phospholipids having different gel–liquid-crystal phase transition temperatures. From their results, Papahadjopoulos et al. (1976), Martin & MacDonald (1976), and Duckwitz-Peterlein et al. (1977) support the first mechanism whereas Kremer et al. (1977) support the second.

We have used a different approach to measure transfer, based on the methods of Doody et al. (1978), Charlton et al. (1976, 1978), and Sengupta et al. (1976), which employ pyrene-labeled lipids. In our case, we have measured the exchange kinetics of 1-palmitoyl-2-pyrenedecanoylphosphatidylcholine (pyrene-PC[2]) between single-walled vesicles of dimyristoylphosphatidylcholine. Our results clearly show that transfer of label takes place through the aqueous phase rather than by vesicle collision. The half-time at 36 °C is 13 h if equilibration of label across bilayers (flip-flop) is negligible; if flip-flop is faster than exchange between vesicles, the half-time is 24 h. A preliminary report of our studies has appeared elsewhere (Roseman & Thompson, 1979). Recently, Galla et al. (1979), using a virtually identical approach, obtained completely different results; they reported that most of the pyrene-PC transfers between dimyristoylphosphatidylcholine and dipalmitoylphosphatidylcholine vesicles with a half-time of ~11 s (23 °C), followed by slow transfer of the remaining probe with a half-time of 8 h (50 °C). The result obtained by Galla et al. (1979) is also in marked disagreement with the results obtained by Martin & MacDonald (1976), Papahadjopoulos et al. (1976), Duckwitz-Peterlein et al. (1977), and Kremer et al. (1977).

Materials and Methods

Dimyristoyl- and dipalmitoylphosphatidylcholines, purchased from Sigma, were purified further by silicic acid column chromatography, acetone precipitation, and extraction with chloroform–methanol–H_2O (8:4:3) containing EDTA. Pyrenedecanoic acid was purchased from Molecular Probes.

1-Palmitoyl-2-pyrenedecanoylphosphatidylcholine was prepared from dipalmitoylphosphatidylcholine according to the method used by Roseman et al. (1978) to prepare 1-palmitoyl-2-oleylphosphatidylcholine. This method, which employs fatty acid anhydrides, contains minor modifications of the procedures developed by Cubero Robles & van den Berg (1969). The absorption and fluorescence spectra of pyrene-PC were identical with those of pyrenedecanoic acid. Galla et al. (1979) found the critical micelle concentration of pyrene-PC to be 10^{-7} M. This is close to the value of 3×10^{-8} M calculated for dimyristoylphosphatidylcholine by Martin &

† From the Department of Biochemistry, University of Virginia School of Medicine, Charlottesville, Virginia 22908. *Received August 9, 1979.* This work was supported by U.S. Public Health Service Grants GM-14628 and GM-23573.
‡ Present address: Department of Biochemistry, Uniformed Services University of Health Sciences, Bethesda, MD 20014.

[1] These references do not include the large number of studies carried out with phospholipid exchange protein on biological membranes, in which the slow uncatalyzed, spontaneous isotopic equilibration of lipids is routinely measured as a control (Shaw et al., 1979).
[2] Abbreviations used: pyrene-PC, 1-palmitoyl-2-pyrenedecanoylphosphatidylcholine.

0006-2960/80/0419-0439$01.00/0